33RD CONGRESS
OF THE INTERNATIONAL COUNCIL
OF THE AERONAUTICAL SCIENCES
STOCKHOLM, SWEDEN, 4-9 SEPTEMBER, 2022

ICAS 2022 SWEDEN

EXPERIMENTAL INVESTIGATION OF THE EFFECT OF THE YAW ANGLE ON THE DRAG REDUCTION RATE FOR TRAPEZOIDAL RIBLETS

Ayumu Inasawa[1], Ryo Taniguchi[1], Masahito Asai[1], Monami Sasamori[2] & Mitsuru Kurita[2]

[1]Department of Aeronautics and Astronautics, Tokyo Metropolitan University, 6-6 Asahigaoka, Hino, Tokyo 191-0065, Japan
[2]Aviation Technology Directorate, Japan Aerospace Exploration Agency

Abstract

Effects of yaw angle of riblets on the drag reducing effect was examined experimentally for riblets having trapezoidal valleys and 30°-ridges with the height-to-span ratio h/s = 0.5 in a turbulent wind channel at Reynolds numbers (based on the friction velocity) Re_τ = 500 – 1900. Drag of riblets was estimated by measurements of streamwise pressure gradient of turbulent channel flows, and the drag reduction rates for yawed riblets of ϕ = 10° and 15° were compared to that for streamwise riblets (ϕ = 0°). Almost the same drag reducing effect as that for the streamwise riblets, $\Delta\tau \approx 7\%$, was observed for the yawed riblets of ϕ = 10°. For ϕ = 15°, however, the maximum drag reduction rate decreased to about 1%. Thus, the drag reducing effect of trapezoidal riblets was more sensitive to the yaw angle than for saw-tooth riblets for which the drag reducing effect was almost the same as that in the streamwise-riblet case even for ϕ = 15°.

Keywords: turbulent flow, drag reduction, riblets, yaw angle effect, turbulent wind channel

1. Introduction

Surface manipulation with riblets (or longitudinal grooves) is one of the most successful passive means to reduce friction drag in wall turbulence. Since early work by Walsh and Weinstein [1] and Walsh [2, 3], several cross-sectional geometries of riblets including triangular, sawtooth, scalloped, blade and trapezoidal ones have been proposed and examined experimentally and numerically [4, 5, 6, 7, 9]. For all the groove geometries of riblets, the drag reducing effect is divided into three regimes. In the viscous regime of $s^+ \leq 10 – 15$, turbulent vortices have no significant impact on the flow inside grooves, and thus the viscous sublayer over the riblets is laminar-like. In this regime, the drag reduction due to a viscous effect is linearly proportional to s^+ [4, 10]. Beyond this value of s^+, the so-called viscous breakdown occurs and drag reducing effect of riblets is saturated at s^+ = 15 – 20 due to increase in the turbulent Reynolds stress near the riblets [11]. Further increasing s^+, the drag reducing effect of riblets is weakened with s^+ (although riblets still affect activity of near-wall turbulence) and finally the friction drag turns to increase (compared to the smooth surface case). The maximum drag reduction rate realized by riblets is thus determined by the viscous effect and viscous breakdown phenomenon, both of which depend on the riblet geometry.

The maximum drag reduction rate was found to be 5% (for triangular riblets) – 10% (for blade riblets) and the optimal size of the riblet cross-section was over 10 – 20 in wall units in terms of the distance between neighboring ridges, depending on the riblet geometry, as summarized in Bechert et al. [8] and García-Mayoral and Jiménez [12]. Here, concerning the optimal riblet size, when the riblet-ridge spacing was represented by the square root of the groove cross-section area in wall units $(A_g^+)^{1/2}$, the maximum drag reduction occurred at $(A_g^+)^{1/2} \approx 10.7 \pm 1$ for all groove geometries [11] .

For application of riblets to aircraft, on the other hand, it is important to understand impacts of yaw angle ϕ (angle between mean flow and riblets) on the drag reducing effects because the drag-reducing

effect may be attenuated by additional pressure drag due to flow separating at riblet-ridges. In this concern, Walsh [13] first examined the yaw effect experimentally for the saw-tooth riblets and reported that the drag reducing effect was not attenuated even for ϕ = 15° and the drag reducing effect was maintained up to ϕ = 20 – 25 although the drag reduction rate started to decrease for ϕ > 15°. The value of ϕ = 15° has often been cited as the critical yaw angle for drag-reduction of riblets. However, no detailed experiment has been conducted for other cross-sectional geometries, especially for riblets with trapezoidal cross section which is expected the larger drag reduction rate than that for triangular riblets, although a direct numerical simulation was conducted for riblets with trapezoidal valleys and 30°-ridges at a low turbulent Reynolds number Re_τ = 180 [14] and reported that the advantage of drag reduction was kept until ϕ exceeded 20° .

In the present study, effects of the yaw angle on the drag reduction rate of riblets are carefully examined for trapezoidal riblets with 30°-ridges experimentally in turbulent wind channel to see how critically the drag reducing effect of riblets is attenuated in off-design conditions. Knowledge of yaw-angle effects of riblets is also important in designing non-straight riblets such as spanwise wavy riblets which could increase the maximum drag reduction by 1 – 2% compared to the straight riblets [15, 16, 17, 18].

2. Experimental setup

The whole experiment was conducted in a turbulent wind channel whose length (L), height ($2H$) and spanwise width (W) were 10 m, 100 mm, and 900 mm, respectively, giving the aspect ratio of the channel cross section of 9. The flow was driven by a counter-rotating axial fan. The center-line velocity U_c can be changed up to about 45 m/s continuously: The maximum bulk Reynolds number defined as $Re_c = U_c H/\nu$ (where ν is the kinematic viscosity) was 1.50 $\times$ 10^5. As for the coordinate system, x was the streamwise distance measured from the channel inlet, y the normal-to-wall distance and z the spanwise distance; see Fig. 1 (a). Both channel walls ($L \times W$ area) were made of transparent and highly-flat-5-mm-thick glass-plates in order to keep the channel cross-section to be constant in the streamwise direction, in addition to the optical access from outside the channel walls. The end walls ($L \times 2H$ area) were of 20-mm-thick Aluminum plate. Note that the channel was set vertically. The channel glass walls were supported rigidly by Aluminum flames attached to the glass walls at an equal interval of 250 mm to avoid wall deformation of the glass walls due to higher static pressure inside the channel than the outside atmospheric pressure; see Fig. 1 (b). The channel had 40 pressure taps (0.4 mm in diameter and 3 mm in depth) with an equal interval of 250 mm in the streamwise direction over 125 mm $\leq x \leq$ 9875 mm. The pressure taps were drilled 225 mm apart from the spanwise mid position (z = 225 mm). To promote transition to fully-developed wall turbulence, the inlet flow was tripped at the channel entrance (x = 200 mm) by gluing two rows of cylinder-roughness elements (height of 5 mm, diameter of 4 mm) in a staggered manner on the both walls in the whole span.

Riblets had triangular ridges with a ridge angle of 30° and trapezoidal valleys. Figure 2 shows schematic diagram and photographs of the trapezoidal riblets used in the experiment. The riblets were manufactured by means of resin mold. The ridge spacing s and height h were 0.83 mm and 0.415 mm (= 0.5s), respectively, giving the ratio of the groove cross-sectional area A_g to the square of the spacing A_g/s^2 = 0.43. Note that the tip thickness of riblet ridges was 0.005 mm. Three riblet-ridge alignments were employed; one was parallel to the mean flow, i.e., streamwise riblets (ϕ = 0°) and the other two were yawed to the mean flow direction, with the yawed angle ϕ = 10° and 15° as shown in Fig. 3. A riblet plate (riblet sheets of 2 m long and 400 mm wide were glued on a 2-m-long glass plate) was connected to the upstream smooth-surface plate in such a way that the bottom of riblet-grooves was placed at the same position as the upstream smooth surface. The virtual origin at which the mean velocity profile approached zero would be about a quarter of riblet height (h/4 $\sim$ 0.1 mm) below the tip of the ridges for streamwise riblets having 30°-ridge and trapezoidal grooves [8]. In such a case, the change in the channel cross sectional area would be only 0.3% of the channel depth ($2H$ = 100 mm) and thus the influence of the surface imperfection would be negligibly small on the comparison of friction drag between the smooth and ribbed surface channels in the present experiment.

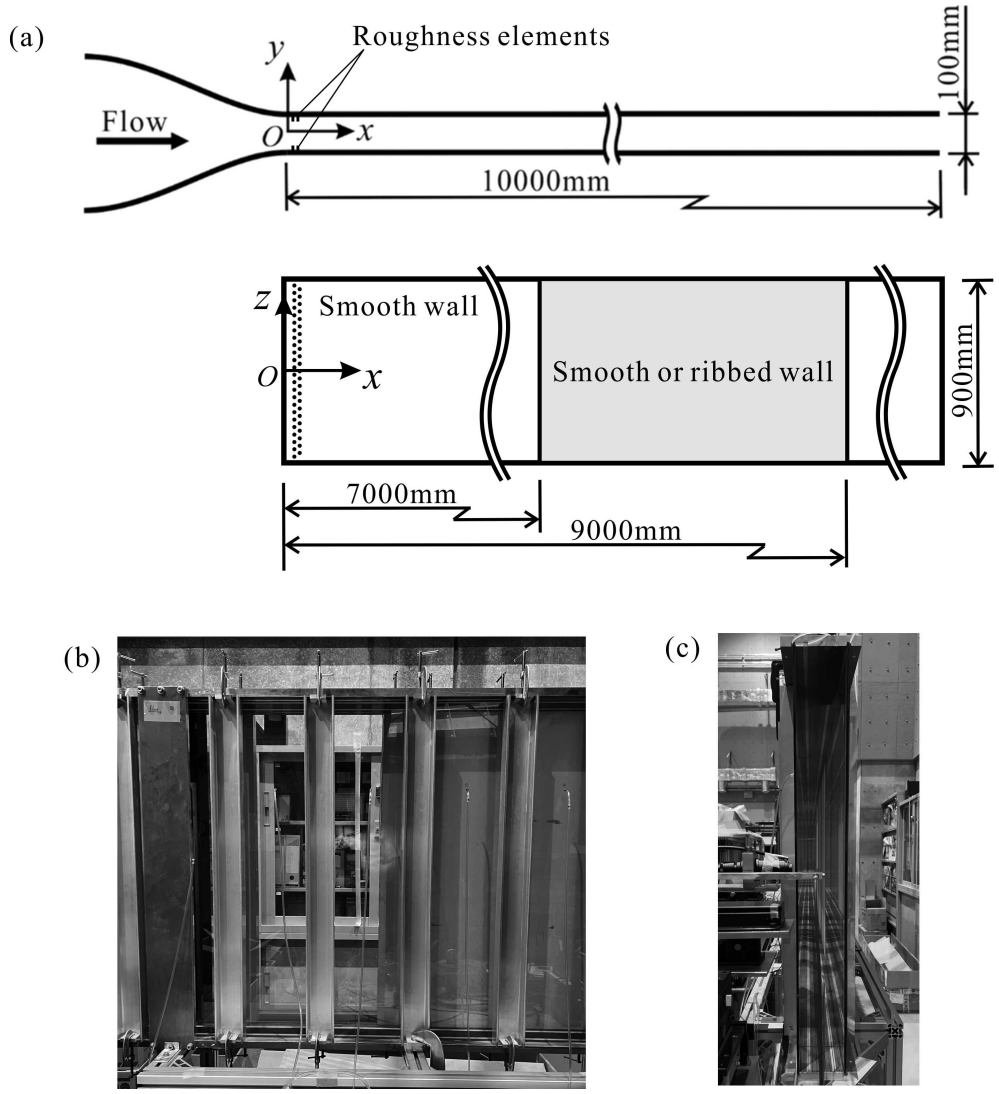

Figure 1 – Turbulent wind channel apparatus. (a) Schematic diagram. (b) Sideview and (c) endview photographs of wind channel with ribbed wall installation in the test section.

Drag reduction rate was obtained by comparing pressure losses (more exactly speaking, the pressure gradient in the streamwise direction) between the smooth and ribbed surfaces in the downstream test section beyond x = 7000 mm. The static pressure was measured using high-precision pressure transducer (Validyne). The output signal was stored in a PC via Analog-to Digital (A/D) converter (NI) with sampling frequency and sampling time being 1000 Hz and 50 s, respectively. In order to minimize the influences of change in kinetic viscosity in a pair of measurements for smooth and ribbed surfaces, temperature and atmospheric pressure in the laboratory was monitored and the center velocity of the channel was set carefully to reproduce the same Reynolds number condition for both cases (with and without riblets). The streamwise velocity component ($U + u$) where U and u denote the time-mean and fluctuation components, respectively was measured using a constant temperature hot-wire anemometer (Pantec). The sensitive length of hot wire (5-μm-tungsten wire) was 1 mm. The hot-wire probe was inserted into the flow from the downstream end of the channel. In order to monitor/measure the sensor position relative to the tip of riblet ridges, a digital microscope (HOZAN) whose working distance from the object to the lens front was 105 mm was employed. The microscope was mounted on a high-precision traversing mechanism with spatial resolution of 0.5 μm (SIGMA). The sensor position could be determined with accuracy within 20μm, about 5% the riblet

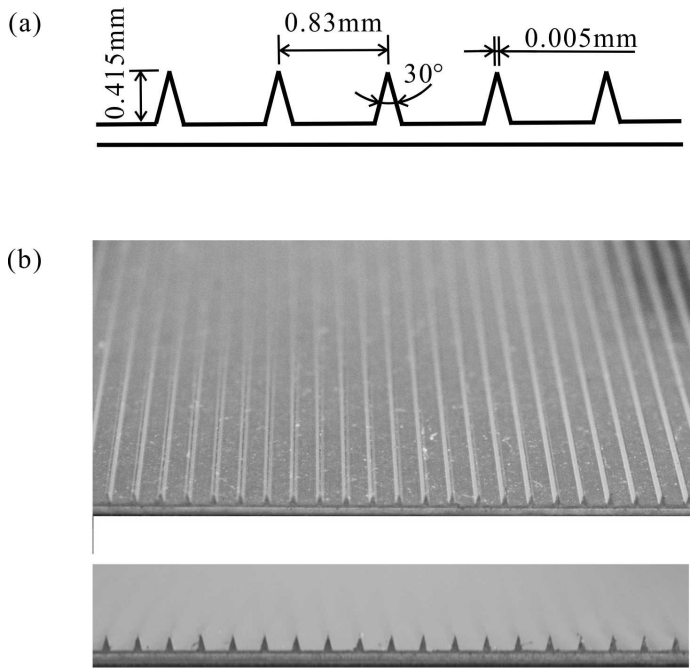

Figure 2 – (a) Schematic diagram of riblet cross-section. (b) Photographs of streamwise riblets.

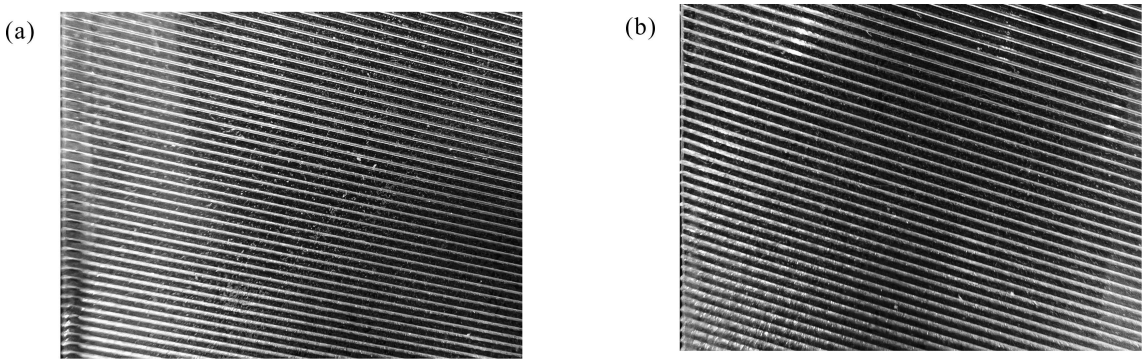

Figure 3 – Photographs of yawed riblets (plan view). (a) ϕ = 10°, (b) ϕ = 15°.The cross-section geometry is the same as that in Fig. 2.

height h, in such a way that the sensor and riblet-edges were respectively in focus. The turbulent Reynolds number based on the friction velocity and channel half width (H = 50 mm) Re_τ ranged over 500 – 1900. The mean streamwise velocity at the channel center U_c was 3 – 13 m/s. The riblet-ridge spacing in wall units $s^+ = su_\tau/\nu$ was less than 31, where u_τ was the friction velocity on the smooth surface.

3. Results and discussion

3.1 Mean flow and streamwise distribution of static pressure

Figure 4 displays streamwise variations of (time-mean) static pressure of flows in the smooth-surface channel at the channel center velocity U_c = 9.87 and 12.5 m/s which gave the Reynolds numbers Re_c = 3.22 $\times$ 10^4 and 4.06 $\times$ 10^4. We see that the pressure gradient has approached a constant value beyond a location about 2000 mm (= 40H) downstream of the inlet for each case. To confirm that the

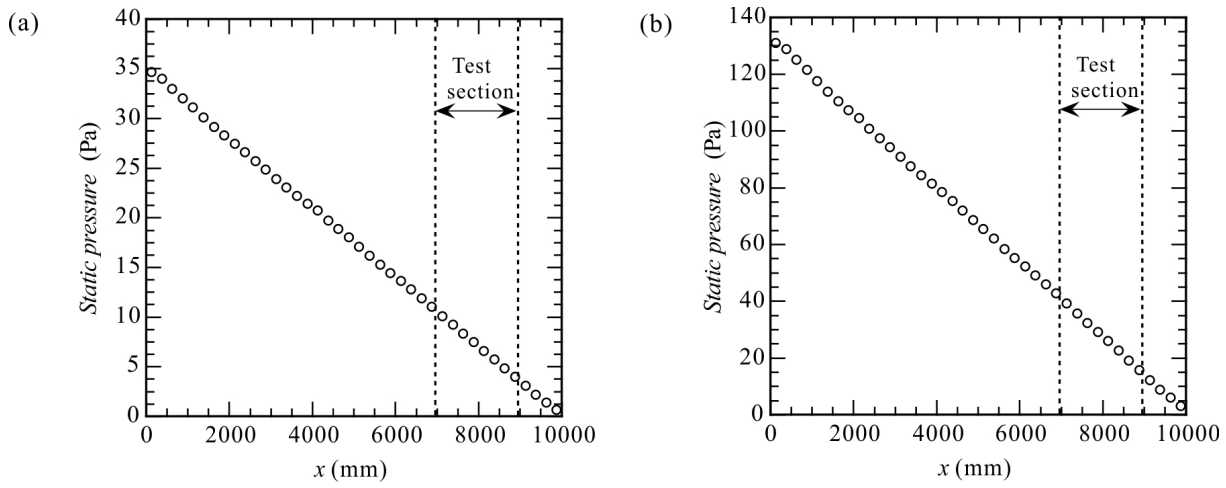

Figure 4 – Streamwise variation of static pressure p in the smooth-surface channel at (a) U_c = 9.87 and (b) 12.5 m/s (Re_c = 3.22 $\times$ 10^4 and 4.06 $\times$ 10^4).

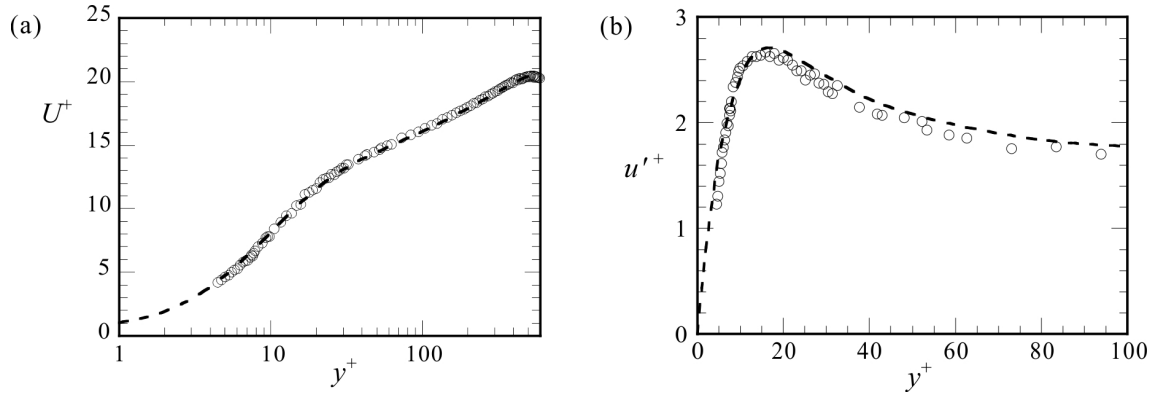

Figure 5 – The y-distributions of (a) mean velocity U and (b) rms value of streamwise velocity fluctuation u' in the smooth-surface channel (Re_τ = 520). Dashed lines represent DNS [19] (Re_τ = 590).

flow is fully developed in the downstream test section, mean flow and rms distributions on the smooth surface were measured at x = 9900 mm. Figures 5(a) and (b) display the y-distributions of mean velocity U and rms value of streamwise velocity fluctuation u', respectively at the turbulent Reynolds number Re_τ = 520, comparing to DNS results [19] made at a close Reynolds number. We see that both U- and u'-profiles agree well with the DNS results, confirming that the turbulent flow tripped by roughness elements was fully developed in the downstream test section. Note that a difference in the y^+-distributions of u'^+ was due to the slight difference in Re_τ.

3.2 Drag reduction rate of streamwise riblets

Figures 6 compares streamwise variations of (time-mean) static pressure of the turbulent channel flows with and without streamwise riblets at Re_τ = 1060 and 1820 (s^+ = 17 and 31 for riblets), respectively. We see a slight difference in the streamwise variation of static pressure between the smooth and ribbed surfaces for Re_τ = 1060 (s^+ = 17 for riblets): The pressure gradient in the riblet case was smaller than that for the smooth-surface case, showing that the turbulent drag was reduced by the

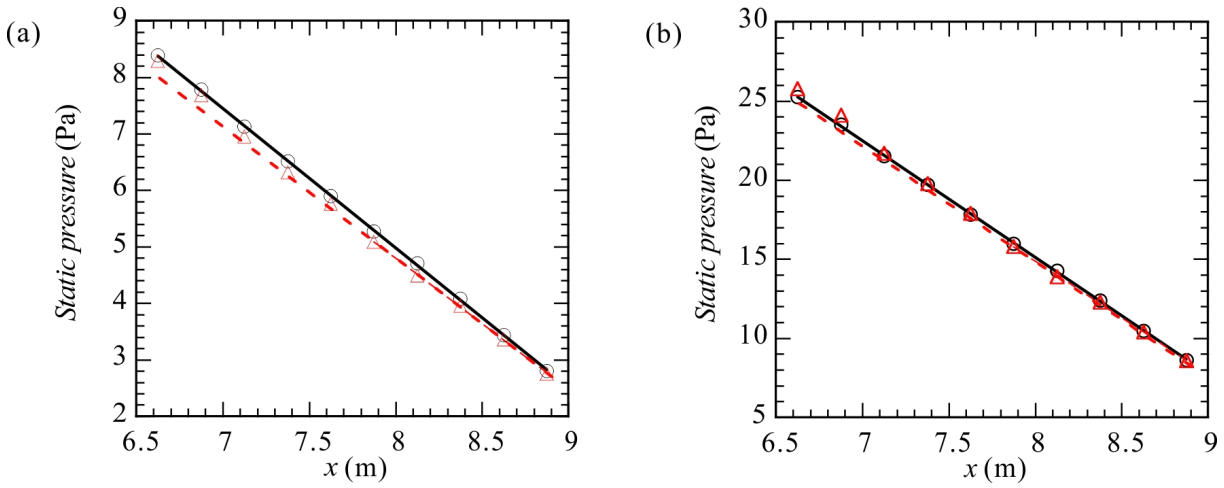

Figure 6 – Comparisons of streamwise variations of static pressure with and without riblets of ϕ =0. Circle (black) and triangle (red) symbols represent smooth and streamwise riblets, respectively. Slope of lines corresponds dp/dx described in text. (a) Re_τ = 1060 (U_c = 7.01 m/s, s^+ = 17 for riblets). (b) Re_τ = 1820 (U_c = 13.1 m/s, s^+ = 31).

riblets. For Re_τ = 1820 (s^+ = 31 for riblets), on the other hand, the pressure gradient was nearly the same between the smooth and ribbed surfaces, indicating that the drag reducing effect disappeared there. Here, it should be noted that the influence of sudden change in the surface geometry (from the upstream smooth surface to the downstream ribbed surface) at x = 7000 mm lasted long downstream, that is, it took a distance of 20H for the pressure gradient to become constant over the riblets. Beyond there, the pressure gradient became constant within measurement accuracy. In this concern, we may refer to an experiment on the downstream influences of a step-like change in rough surface in a turbulent pipe flow [20], in which the pressure gradient attains the equilibrium state about 20 radii downstream of the step change. The distance is the same as that in the present experiment ($\sim 20H$). Therefore, in the present experiments, streamwise variations of static pressure over 8125 mm $\leq x \leq$ 8875 mm (distance of four pressure taps) were adopted to evaluate the turbulent drag of the ribbed surface τ_{riblet}, while the pressure distributions over 7375 mm $\leq x \leq$ 8875 mm (seven pressure taps) were used to obtain the turbulent drag for the smooth surface τ_{smooth}. Note that the pressure gradient dp/dx was obtained by the 1st order least-square method for the measured pressure data.
The drag reduction rate $\Delta\tau$ was defined as,

$$\Delta\tau = \frac{\tau_{\mathrm{riblet}} - \tau_{\mathrm{smooth}}}{\tau_{\mathrm{smooth}}} \tag{1}$$

where the friction stress on the smooth surface τ_{smooth}, averaged over the 4 plate surfaces, was given as $(9H/10)(dp/dx)_{\mathrm{smooth}}$ since W = 18H, and $\tau_{\mathrm{riblet}} - \tau_{\mathrm{smooth}}$ was obtained from the difference in the measured pressure gradient between the riblet-surface and smooth-surface cases, assuming that the shearing stress is the same as that for the smooth-surface channel except the ribbed surface,

$$\tau_{\mathrm{riblet}} - \tau_{\mathrm{smooth}} = 2H\left[\left(\frac{dp}{dx}\right)_{\mathrm{riblet}} - \left(\frac{dp}{dx}\right)_{\mathrm{smooth}}\right] \tag{2}$$

In the comparison of drag reduction rate between the smooth surface and riblets, the wall units (u_τ and ν/u_τ) were defined with the friction velocity measured on the smooth surface. Figure 7 depicts the drag reduction rates $\Delta\tau$ against the riblet spacing s^+ for the streamwise riblets (ϕ = 0°). The

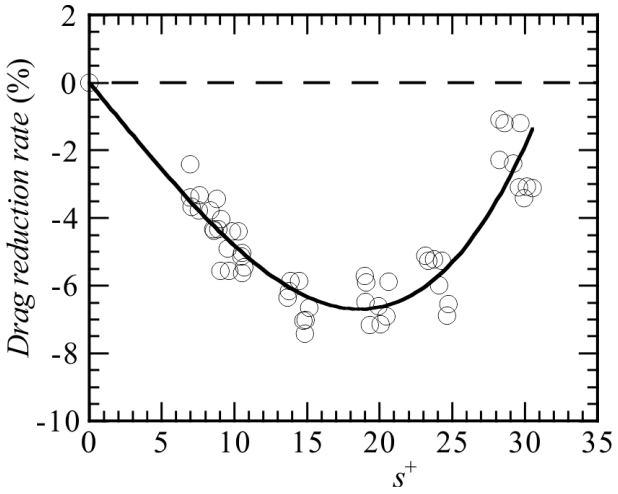

Figure 7 – Drag reduction rate $\Delta\tau$ versus riblet spacing (in wall units) s^+ for streamwise riblets. The measurements (over $s^+ \approx 7 - 30$) were conducted more than 5 times. Solid lines represent regression curves for measured data.

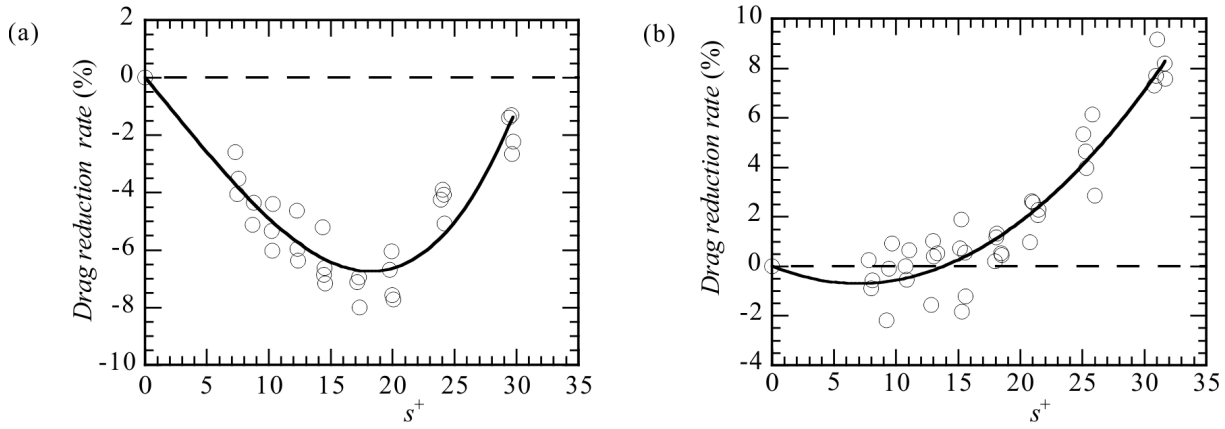

Figure 8 – Drag reduction rate versus riblet spacing s^+ (in wall units) for yawed riblets. (a) $\phi = 10°$, (b) $\phi = 15°$. The measurements were conducted more than 4 times in both cases. Solid lines represent regression curves for measured data.

measurement was carried out more than 5 times for each s^+ and the regression curve was obtained for the measured data using a cubic polynomial. The maximum drag reduction rate defined by Eq. (1) was about 7% for s^+= 18 and the drag reduction was observed for $s^+ \leq 30$ (Fig. 7). This result is well correlated with that reported by Bechert et al. [8] where the drag force was measured directly using a balance. It is also noted that the root of the groove cross section $(A_g^+)^{1/2}$ was 11.8 for s^+ = 18, which was close to the optimal value 10.7$\pm$1 [12].

3.3 Effects of yaw angle of trapezoidal riblets on drag reduction rate

We replaced the streamwise-riblet plate to the yawed riblet plates and repeated measurements of the drag reduction rates similarly. Figs. 8 (a) and (b) depict the drag reduction rates ($\Delta\tau$) against the riblet spacing (s^+) for ϕ = 10° and 15°, respectively. For the yawed riblets of ϕ = 10° in Fig. 8 (a), the maximum drag reduction rate was about 7% at $s^+ \approx 18$ and the drag reduction effect of riblets was

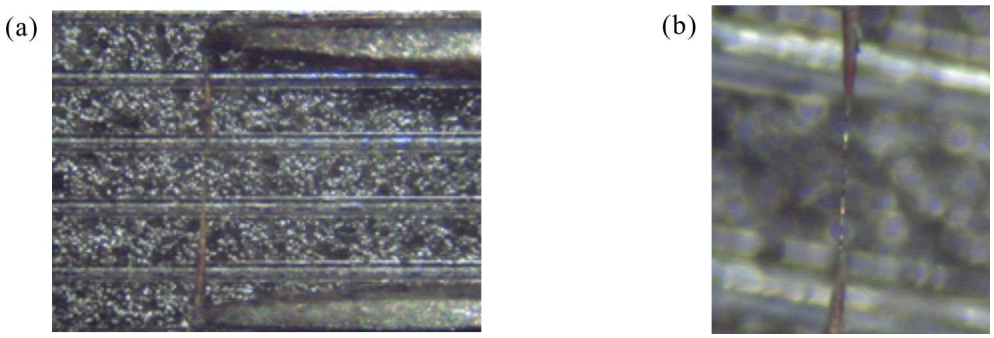

Figure 9 – Photograph of hot-wire sensor just above (a) streamwise riblets (ϕ = 0°) and (b) yawed riblets of ϕ = 15°. The position of hot-wire sensor (diameter of 5 μm) was 0.85 mm from the tip of ridges in (b).

preserved up to $s^+ \approx 30$, which was the same as that observed for the streamwise riblets. Thus, the drag reducing effect was still preserved without notable increase of pressure drag at least up to this yaw angle. For ϕ = 15°, on the other hand, the drag reduction rate decreased drastically to at most 1 – 2% (at around $s^+ \approx 10$) and the riblets worked as distributed roughness for $s^+ \geq 15$. In this concern, we should refer to the early experiment by Walsh [13] in which the yaw angle effect was examined for saw-tooth (triangle) riblets with ridge angle of 90°. In his experiment, the drag reducing effect did not attenuate even at ϕ = 15° and the drag reduction occurred up to $\phi \approx 25°$.

The difference in the yaw angle effect between the triangular and trapezoidal riblets can be attributed to the fact that the flow separation would be easier to occur at the riblet-ridges for the trapezoidal riblets with ridge angle of 30° when the ridge alignment is inclined to the main flow direction. To confirm this, we examined the velocity profiles very close to the surface of yawed riblets carefully using a hot-wire anemometer. Figures 9 (a) and (b) are photographs of the hot-wire sensor very close to streamwise riblets and yawed riblets, respectively. Our attention was paid to a close comparison of the mean velocity profiles near the riblets between ϕ = 10° and 15° in Fig. 10 (a) and (b); Fig. 10 (b) is a close-up of the profiles near the riblets ($y - y_{\mathrm{tip}} \leq 4$ mm). The comparison was made with the same s^+ condition, s^+ = 15 where the drag reduction rate was close to the maximum for $\phi = 0°$ and 10°, while the drag had already turned to increase at s^+ = 15 for ϕ = 15°. The comparison clearly shows that the virtual origin where U tended to zero was located inside the grooves for ϕ =10°, while it was near the tip of riblet-ridge for ϕ = 15°. This no doubt indicates that the pressure drag caused by flow separation at the riblet-ridges increased and cancelled out the reduction of friction drag for ϕ = 15°. In Fig. 10 (c) and (d), we compare the y-distributions of the rms value u' near the riblets between ϕ = 10° and 15°. The maximum rms values were not so different between these two case and were smaller than that for the smooth surface case. Thus, the drag reduction rate was attenuated despite the yawed riblets could suppress the turbulent intensity even for ϕ = 15°. Only a distinct difference is that the peak for ϕ =15° was only slightly shifted toward higher y-position, corresponding to the change of the virtual origin observed in the velocity profile.

4. Conclusion

Effects of the yaw angle of riblets on the drag reduction rate were examined experimentally using a turbulent wind channel for the trapezoidal riblets with ridge angle of 30°. The maximum drag reduction rate was about 7% at around $s^+ \approx 18$ for the streamwise riblets. The drag reducing effect did not attenuate up to ϕ = 10°. When the yaw angle increased to 15°, flow separation occurred at the riblet ridges so that the drag reduction rate decreased drastically down to 1 – 2%, which was much different from the saw-tooth-riblet case reported by Walsh [13] where the drag reducing effect did not attenuate at all even for ϕ = 15° and was observed up to ϕ = 25°. Thus, the yaw angle effect of riblets is highly dependent on the riblet cross-section geometry. Further experiments on the yaw

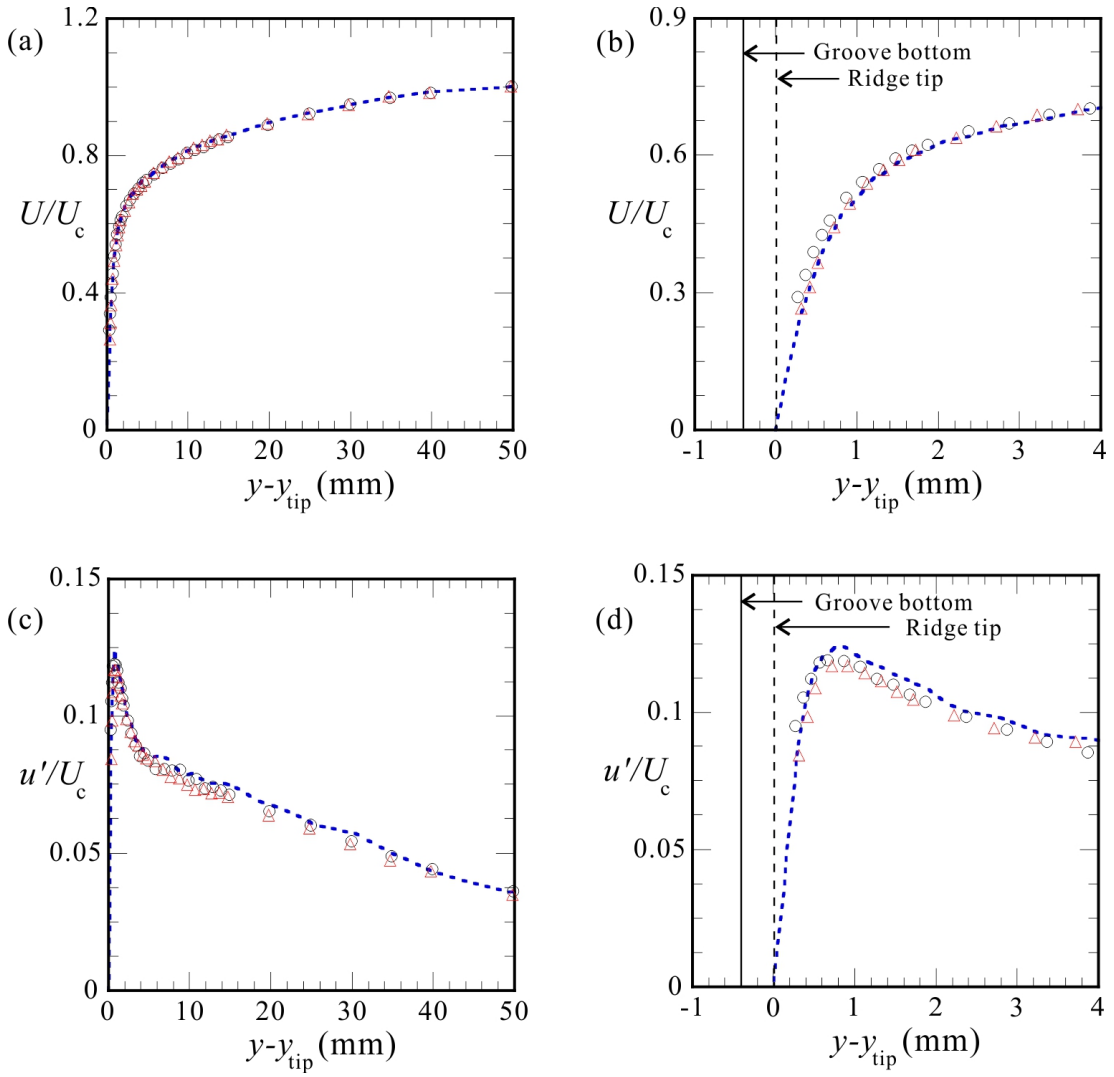

Figure 10 – Comparison of the y-distributions of (a, b) mean velocity U and (c, d) rms value u' near the riblets between ϕ = 10° (circle) and 15° (triangle) at s^+ = 15 (Re_τ = 900). Dotted lines represent distributions in the smooth surface case at the same Reynolds number.

angle effect are in progress including riblets with other cross-section geometry.

Acknowledgments

This work was supported by JSPS Grant-in-Aid for Scientific Research (19H02350) and Research Grant from JAXA.

Copyright Statement

References

[1] Walsh M J, Weinstein L M. Drag and heat transfer of surface with small longitudinal fins. *AIAA Paper* 78–1161, 1978.

[2] Walsh, M. J. Drag characteristics of V-groove and transverse curvature riblets. In *Progress in Astronautics and Aeronautics* , 72 (ed. G. R. Hough), AIAA, pp. 168–184, 1980.

[3] Walsh M.J. Riblets as a viscous drag reduction technique, *AIAA J.* Vol. 21, No. 4, pp. 485-486, 1983.

[4] Bechert D. W., Bartenwerfer M. 1989 The viscous flow on surfaces with longitudinal ribs. *J. Fluid Mech.* Vol. 206, pp. 105-129, 1989.

[5] Choi K.-S. Near-wall structure of a turbulent boundary layer with riblets, *J. Fluid Mech.* Vol. 208, pp. 417-458, 1989.

[6] Walsh M. J. Viscous Drag Reduction in Boundary Layers. In *Progress in Astronautics and Aeronautics*, Vol. 72 (eds. D. M. Bushnell and J. N. Hefner), AIAA, pp. 203–261, 1990.

[7] Choi H., Moin P., Kim J. Direct numerical simulation of turbulent flow over riblets. J. Fluid Mech. Choi, H.,Moin, P. and Kim, J. 1993 Direct numerical simulation of turbulent flow over riblets. *J. Fluid Mech.* Vol. 255, pp. 503-539, 1993.

[8] Bechert D W, Bruse M, Hage W, Van Der Hoeven J G T and Hoppe G. Experiments on drag-reducing sur faces and their optimization with an adjustable geometry. *J. Fluid Mech.*,Vol. 338, pp. 59-87, 1997.

[9] Suzuki Y., Kasagi N. Turbulent drag reduction mechanism above a riblet surface. *AIAA J.*, Vol. 32, No. 9, 1994.

[10] Luchini P., Manzo F., Pozzi A. Resistence of a grooved surface to parallel flow and cross-flow. *J. Fluid Mech.*, Vol. 228, pp. 87–109, 1991.

[11] García-Mayoral R and Jiménez J. Hydrodynamic stability and breakdown of the viscous regime over riblets. *J. Fluid Mech.* Vol. 678, pp. 317–347, 2011.

[12] García-Mayoral R and Jiménez J. Drag Reduction by riblets. *Phil/ Trans. Roy. Soc.* A, Vol. 369, pp. 1412–1427, 2011.

[13] Walsh M. J. Turbulent boundary layer drag reduction using riblets. *AIAA-paper* 82–0169, 1982.

[14] Okabayashi K. Direct numerical simulation for investigation on yaw angle effects on riblets. *Transactions of Japan Society of Mechanical Engineers*, Vol. 12, No. 1, JSFT0008, 2017.

[15] Peet Y., Sagaut P. Theoretical prediction of turbulent skin friction on geometrically complex surface, Phys. Fluids, Vol. 21, 105105, 2009.

[16] Sasamori M., Mamori H., Iwamoto K., Murata A. Experimental study on drag-reduction effect due to sinusoidal riblets in turbulent channel flow. *Exp. Fluids*, Vol. 55, 1824, 2014.

[17] Okabayasi K., Yamada Y., Asai M. Parametric analysis of flow over sinusoidal riblets. *Proc. TSFP-9*, No. 237, 2015.

[18] Sasamori M., Iihama O., Mamori H., Iwamoto K. Parametric study on a sinusoidal riblet for drag reduction by direct numerical simulation. *Flow, Turbulence and Combustion*, Vol. 99, pp. 47-69, 2017.

[19] Moser R D, Kim J, Mansour N N. Direct numerical simulation of turbulent channel flow up to Re_τ =590. Phys. Fluids, Vol. 11, No. 4, pp. 943–945, 1999.

[20] Van Buren T., Floryan D., Ding L., Hellstrom L. H. O, Smits A. J. Turbulent pipe flow response to a step change in surface roughness. *J. Fluid Mech.*, Vol. 904, 2020.